lubricants

MDPI

Article

Wear of Stellite 6 Coatings Produced with High-Velocity Oxygen Fuel at Elevated Temperatures

Alejandra Islas Encalada [1], Pantcho Stoyanov [2], Mary Makowiec [3], Christian Moreau [4] and Richard R. Chromik [1,*]

[1] Department of Mining and Materials Engineering, McGill University, M.H. Wong Building, 3610 University Street, Montreal, QC H3A 0C5, Canada; alejandra.islasencalada@mail.mcgill.ca
[2] Department of Chemical and Materials Engineering, Concordia University, EV Building, 1515 St. Catherine W., Montreal, QC H3G 2W1, Canada; pantcho.stoyanov@concordia.ca
[3] Pratt & Whitney, 400 Main Street, East Hartford, CT 06118, USA; mary.makowiec@prattwhitney.com
[4] Department of Mechanical, Industrial and Aerospace Engineering, Concordia University, EV Building, 1515 St. Catherine W., Montreal, QC H3G 2W1, Canada; christian.moreau@concordia.ca
* Correspondence: richard.chromik@mcgill.ca

Abstract: This paper investigates the tribological behavior of Stellite 6 coatings produced with high-velocity oxygen fuel (HVOF), with an emphasis on the transition between severe and mild wear regimes and the glaze layer formation. The development of these coatings involved two spray parameters modifying the oxygen fuel ratio and three post-heat treatment conditions at temperatures ranging between 600 °C and 1150 °C. The coatings were tested under conditions varying the normal load, temperature, sliding distance, and testing temperatures (up to 300 °C). The results show that the coating obtained from the HVOF process exhibited a microstructure different from the conventional bulk Co-alloys, significantly impacting the wear performance. The coating post-processing was essentialto enhance wear resistance at elevated temperatures.

Keywords: Stellite 6; glaze layer; HVOF; coatings; wear; elevated temperature

check for updates

Received: 12 May 2025
Revised: 4 June 2025
Accepted: 9 June 2025
Published: 15 June 2025

Citation: Encalada, A.I.; Stoyanov, P.; Makowiec, M.; Moreau, C.; Chromik, R.R. Wear of Stellite 6 Coatings Produced with High-Velocity Oxygen Fuel at Elevated Temperatures. *Lubricants* **2025**, *13*, 264. https://doi.org/10.3390/lubricants13060264

Copyright: © 2025 by the authors. Licensee MDPI, Basel, Switzerland. This article is an open access article distributed under the terms and conditions of the Creative Commons Attribution (CC BY) license (https://creativecommons.org/licenses/by/4.0/).

1. Introduction

Co-based alloys exhibit exceptional wear and corrosion resistance, making them suitable for diverse high-performance applications [1,2]. These alloys are frequently used as coatings, as they can be applied to various substrates to enhance surface properties [3]. The primary alloying element in Co-based alloys is chromium, which enhances their exceptional resistance to oxidation and corrosion [1,4]. These alloys are further strengthened by elements such as carbon, tungsten, or molybdenum through solid solution or the formation of intermetallic compounds [5]. Examples of cobalt-based alloys include Haynes, Stellites, and Tribaloys [6]. The wear mechanisms in Co-based alloys shift from severe to mild above a transition temperature, with several studies reporting a transition as low as 250 °C [7,8]. Compared with most other materials, this transition to mild wear is an advantage of Co-based alloys, where wear is generally detrimental at higher temperatures due to oxidation and thermal softening.

While extensive research has investigated the conditions that facilitate mild wear and the formation of protective tribolayers (glaze layers), most studies have focused on bulk materials at temperatures above 500 °C [5,7–25]. Fewer investigations have examined the impact of tribolayers on coatings [26–32]. Stellite 6 coatings produced by HVOF have demonstrated microstructural differences (such as the presence of pores, oxidation and

splat boundaries) that differ from those observed in bulk-cast materials (i.e., the presence of intermetallics, elemental distribution related to cast-solidification), which have an impact in properties such as corrosion resistance and wear performance [3,5,31].

To further understand the wear behavior of Co-based alloy coatings, this study evaluated various wear conditions at 300 °C; the goal was to identify the key parameters driving the transition from severe to mild wear in these Stellite 6 coatings produced by HVOF.

2. Materials and Methods

Stellite® 6 powder (Eutectic Powders, Vaudreuil-Dorion, QC, Canada), with a nominal particle size D_{v50} of 34 µm, was used to spray the coatings. The coatings were applied at the parameters listed in Table 1, with an Oerlikon Metco Diamond Jet™ 2700 gun (Westbury, NY, USA) for HVOF spraying. Condition A refers to the standard condition [33]; Condition B was a fuel-rich condition designed to use all available oxygen and reduce the oxidation of the splats and oxides in the coating after spraying [34]. A D8 Discovery diffractometer (Bruker, Billerica, MA, USA) equipped with a cobalt source (λ = 1.78897 Å) was used to analyze the structure of the powder and the as-sprayed coating. The coatings were prepared for observation and testing following a standard metallographic procedure of grinding with SiC papers and three steps of polishing using 9, 3, and 1 µm diamond solution. Micrographs and elemental analysis were obtained from the cross-section using a scanning electron microscope (SEM, SU3500 and SU8500, Hitachi, Minato-ku, Tokyo, Japan) equipped with an EDS detector.

Table 1. Spraying conditions.

Parameter	A	B
Powder feed rate (g/min)	23	23
Oxygen flow rate (LPM)	304	152
Propylene flow rate (LPM)	79	87
Air flow rate (LPM)	422	331
Spraying distance (mm)	150	150
Transverse speed (mm/s)	1000	1000
Number of passes	25	25
Width of spray (mm)	3	3

Spray coatings were tested under reciprocating sliding using a TRB (Anton Paar, Baden, Switzerland) against an alumina ball of 6.35 mm diameter and following the metallographic preparation mentioned above. Table 2 details the wear testing conditions, including a 10 mm track length and 1 Hz frequency. For conditions without heat treatment, stainless steel was used as the substrate, while a Ni alloy (X750) was used for heat-treated conditions. Unless otherwise stated, only one test was performed per condition. The wear rate was determined by estimating the volume loss of the wear tracks using profilometry NewView (Zygo Corporation, Middlefield, CT, USA). A minimum of 25 profiles were measured to calculate the average and standard deviation of the area under the curve. The wear rate values were normalized using each condition's track length, load, and distance.

The protective glaze layers found on Stellite 6 and similar cobalt alloys are tribolayers that develop over time through tribo-sintering, a compaction process that arises from the contact stresses and high temperatures generated by sliding wear [17,35,36]. Therefore, variations in temperature (condition 2), applied load (conditions 3 and 4), and distance (proportional to time, conditions 5 to 8) were included in this study. Heat treatments (conditions 9 to 11) were performed on polished coatings in a Lindberg/Blue furnace in ambient air, followed by air cooling or water quenching, simulating wear and oxidation tests from the literature, at 600 °C for 2 h (air cooled), 850 °C for 24 h (air cooled), and

1150 °C for 1 h (water quenched). Wood et al. [19] demonstrated that at 600 °C, glaze layer coverage increased from 60% to 90% between 1 and 3 h. Bolelli et al. [28] found improved wear resistance in a Co-based coating after a 600 °C heat treatment for 1 h, leading us to select 2 h for the first heat treatment. Studies on a similar Co-based alloy (Haynes 25) showed that pre-wear heat treatments above 1000 °C enhanced mechanical properties with minimal oxidation, guiding the second heat treatment [13,17]. These conditions were also used for solution annealing [37]. Lastly, we chose 850 °C for 24 h to promote surface oxidation, a relatively low temperature and short duration compared with typical oxidation tests [38]. All heat treatments and wear tests were conducted under ambient laboratory air, without humidity or oxygen control.

Table 2. Wear test conditions.

Parameters	Spray	Temperature (°C)	Load (N)	Distance (m)	Heat Treatment (°C-h)
Std	A	300	5	400	none
1	B	300	5	400	none
2	A	100	5	400	none
3	A	300	1	400	none
4	A	300	10	400	none
5	A	300	5	100	none
6	A	300	5	800	none
7	A	300	5	1600	none
8	A	300	5	3200	none
9	A	300	5	400	600-2
10	A	300	5	400	850-24
11	A	300	5	400	1150-1

The highlighted parameters show the differences from the standard conditions.

The microstructure of the as-sprayed coating, as well as the analysis of the wear track, were evaluated using scanning electron microscopy. The tribolayer formed after wear was then sectioned for post-analysis using a focused ion beam microscope (FIB, SU-8230, Hitachi, Minatoku, Tokyo, Japan) and analyzed with scanning transmission electron microscopy (STEM, Talos F200X G2, Thermo Scientific, Waltham, MA, USA).

3. Results and Discussions

Section 3.1 presents a detailed description of the feedstock powder, the as-sprayed coating microstructure, and the impact of these on the mechanical properties. The wear performance of the coating under standard (Std) test conditions is also discussed, focusing on the coefficient of friction and wear rate observed.

Section 3.2 then examines the effects of varying the spraying and testing parameters on the wear behavior of the coating, as summarized in Table 2. This section will explore how changes to the spraying process, test temperature, load, distance, and heat treatment can influence the coating's friction and wear characteristics.

3.1. Coating Characterization of Standard (Std) Condition

The standard (Std) condition served as the benchmark for comparison with the different testing conditions examined in the following section, with the spraying parameters defined as "condition A" in Table 1. These spray parameters resulted in a 326 ± 14 µm thickness coating composed of a mixture of molten and semi-molten Stellite 6 splats, with distinct oxide regions forming at the splat boundaries, as observed in the microstructural analysis shown in Figure 1. The formation of these oxide regions can be attributed to the high-velocity oxy-fuel deposition process, which introduced significant thermal energy and

oxygen exposure during spraying. The particle size distribution and detailed micrographs of the cross-section of a powder particle and the resulting coating, obtained using electron channeling contrast imaging, are presented in Figure 2. The Stellite® 6 powder (Figure 2a–c) was produced by atomization. It exhibited a characteristic dendritic structure, with cobalt being the predominant element within the dendrites (point 2) and chromium concentrated more on the outside (point 1). This elemental segregation in the powder was a result of the atomization process. In contrast, the coating microstructure was marked by a refined grain structure compared with the starting powder, a consequence of the rapid solidification and high cooling rates experienced during HVOF deposition (Figure 2d–f). X-ray diffraction (XRD) analysis of the powder feedstock and the as-spray coating presented three main peaks characteristic of the metastable FCC structure, confirming no phase transformation during the coating deposition (Figure 3).

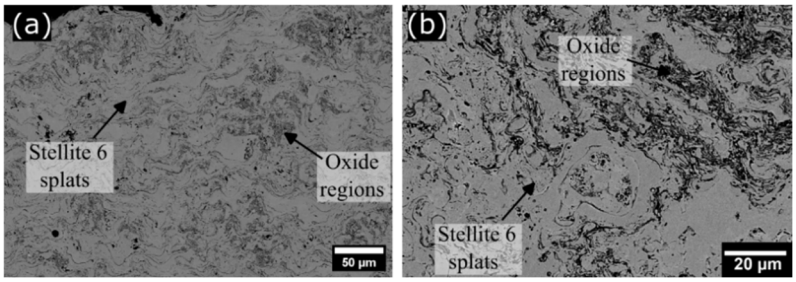


Figure 1. Stellite 6 coating produced with spraying parameters following condition A, (**a**) cross-section, (**b**) top section.

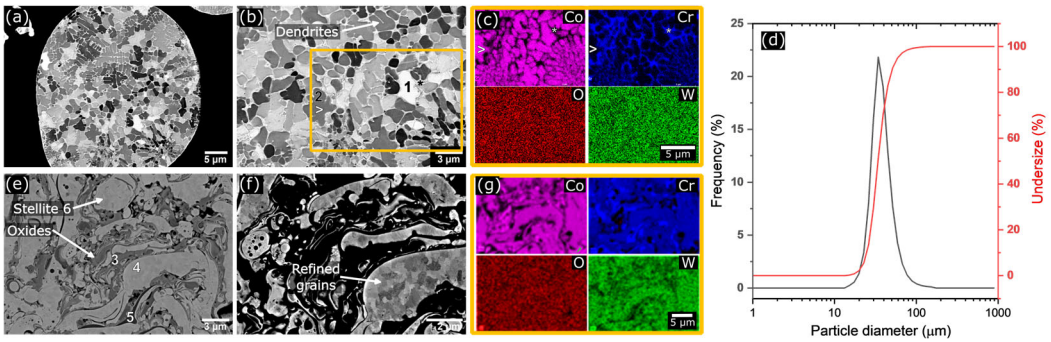


Figure 2. Cross-section of Stellite 6 powder, (**a**) low magnification, (**b**) high magnification, and (**c**) EDS-mapping of selected region from b (marks > and * point the core or outer dendrite region, respectively, in the different element mapping). Cross-section of as-sprayed coating taken with (**e**) BSE signal and (**f**) ECCI, (**g**) EDS mapping of the f-region. Particle size distribution of the powder feedstock (**d**). EDS point analysis of points 1 to 5 are presented in Table 3.

Elemental analysis (Table 3) confirmed the heterogeneous distribution of elements across the Stellite 6 powder particles. Within the dendritic microstructure of the powder, a larger cobalt-to-chromium ratio was observed in the dendrite cores (point 2) compared with the outer regions (point 1). In contrast, the chemical composition of the Stellite 6 splats of the coating (point 4) was closer to the nominal alloy composition (60Co, 30Cr, 5W wt.%), as the high-velocity oxy-fuel deposition process homogenized the elemental distribution during the rapid melting and solidification of the powder particles. However, the oxide-rich regions at the splat boundaries were enriched in chromium (points 3 and 5), exhibiting a Co/Cr ratio of 1 or lower.

Table 3. Chemical composition measured with SEM-EDS point analysis of selected regions.

Element	1	2	3	4	5	6
Co	49	69	33	61	12.5	Co
Cr	38	25	33	29	49.5	Cr
W	5	2	3	3.5	0.5	W
C	8	4	3	6	3.5	C
O	-	-	28	0.5	34	O

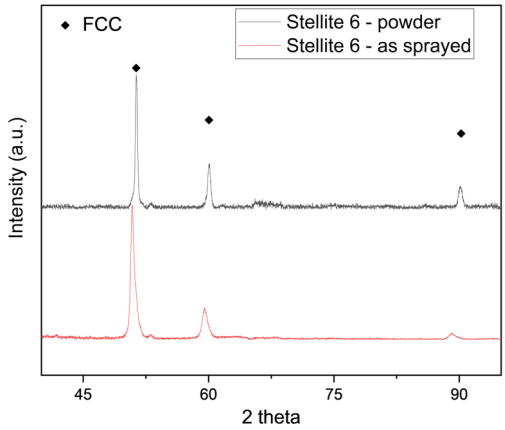


Figure 3. XRD spectra of powder feedstock and coating as sprayed.

The wear performance of the coating was evaluated under the standard test conditions (Std, Table 2), which can be summarized as 300 °C, 5 N normal load, 10 mm stroke length, 3.14 cm/s sliding speed, 1 Hz frequency, and a total distance of 400 m on a polished sample with a roughness average of 0.04 µm without any prior heat treatment. The coefficient of friction data are plotted in Figure 4, showing the results for two replicate tests under the standard conditions. The average CoF values were 0.57 ± 0.06 and 0.51 ± 0.06 for the Std1 and Std2 conditions, respectively, indicating a relatively high and variable coefficient of friction. The CoF values were observed to extend from 0.34 up to 0.74 over the 400 m sliding distance, suggesting significant variation in the frictional behavior during the test. The measured wear rates were 174 ± 9 and 152 ± 3 × 10^{-6} mm^3/N·m for the Std1 and Std2 conditions, respectively, demonstrating a moderate level of wear under these standard test parameters.

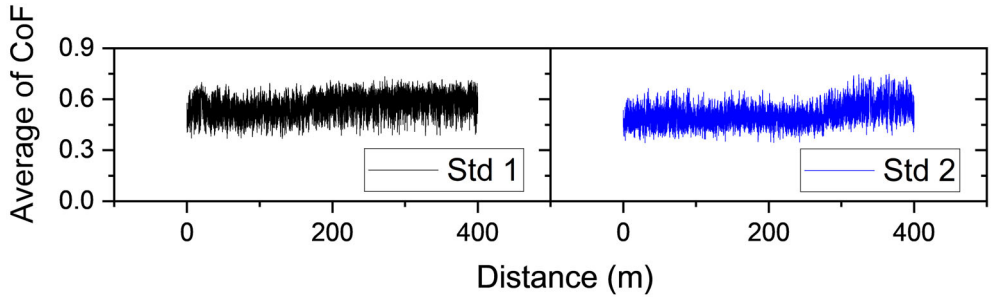


Figure 4. CoF of Std condition.

3.2. Effect of Parameters on CoF and Wear

The conditions presented in Table 2 evaluated the effects of various parameters, including spraying parameters, testing temperature, maximum load, total sliding distance, and heat treatment. The average coefficient of friction is plotted in Figures 5 and 6. Friction coefficients for most conditions were similar to the standard conditions, exhibiting values

between 0.39 and 0.76 across all testing. Low CoF values were observed only after the coating was heat-treated above 800 °C, indicating that the heat treatment significantly impacted the frictional behavior of the coating. Figure 7 shows the statistical values per condition, with the reference lines fixed to the values obtained from the standard conditions. The wear rate of the different conditions is also plotted in Figure 7. Five conditions exhibited a wear rate below that of the Std1 conditions, demonstrating that certain parameter variations improved the wear resistance of the coating. The Std2 conditions also demonstrated variability between multiple repeats under the same conditions, highlighting the importance of assessing the consistency of the coating's performance. The testing at 100 °C showed a lower wear rate, likely due to the thermal softening of the material, which may have reduced its resistance to wear [33]. Conditions 6, 7, and 8 also had lower wear rates. Even though the wear rate is a normalized value, the volume loss may not necessarily increase linearly with distance or time if protective tribolayers are formed. Finally, the condition with the lowest wear rate was condition 11, representing 2% of the value obtained from Std1; these conditions corresponded to a sample heat-treated at 1150 °C, indicating that the high-temperature heat treatment had a significant impact on improving the wear resistance of the coating.

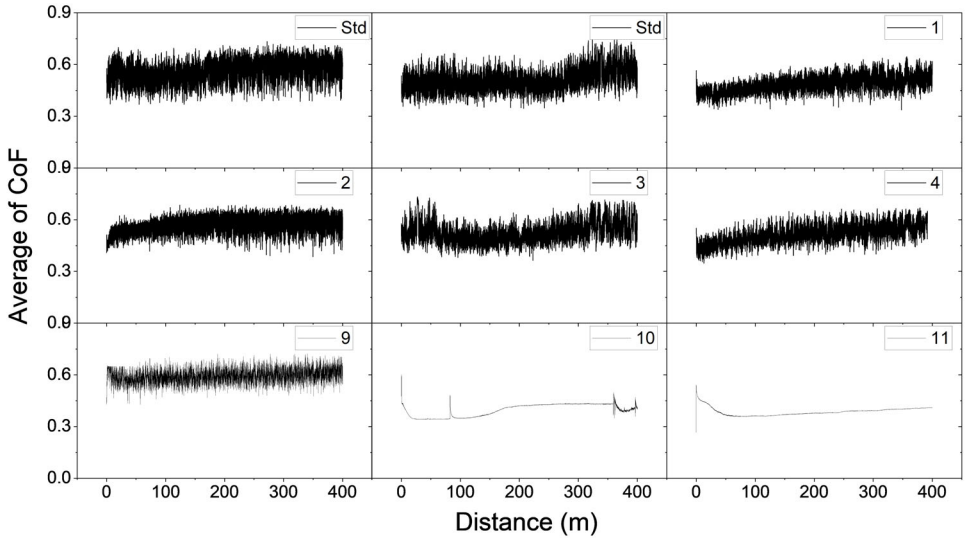


Figure 5. Average CoF of conditions described in Table 2.

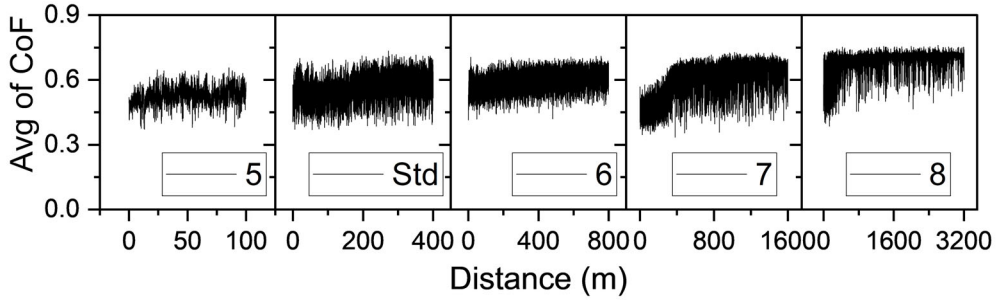


Figure 6. Average CoF with different total distance.

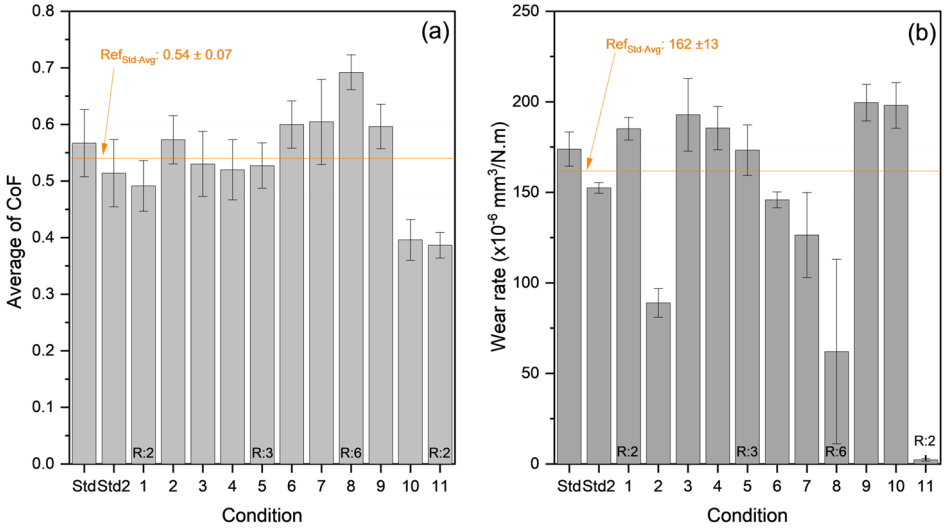


Figure 7. (**a**) Average CoF and (**b**) wear rate per condition. Straight lines show the reference value taken from the average value of the Std conditions. The numbers of repeats per condition are represented by the R value.

3.3. Wear Mechanisms

Conditions 1 up to 10, similar to the standard conditions, exhibited mainly abrasive and oxidative wear, where the oxide regions formed tribolayers with rough and smooth appearances. Figure 8 shows the top surface of the wear track of the Std condition as an example of the general wear mechanism. The heat treatment used for condition 10 produced oxides that covered the surface, which were then removed by abrasive wear, creating a small wear track that exposed the underlying metallic coating (Figure 8). This exposure of the metallic coating suggests that the heat-treatment-induced oxides were easily removed during the wear testing. In contrast, the heat treatment used for condition 11 resulted in a thin and shallow wear track with smeared oxides, differing from the previous conditions. The smeared oxide morphology implies a more stable and protective compacted oxide tribolayer formed during the wear test under these heat-treated conditions. The following sections discuss the differences between each condition and the standard condition, providing further insights into the role of heat treatment and its impact on the wear mechanisms of the Stellite 6 coatings.

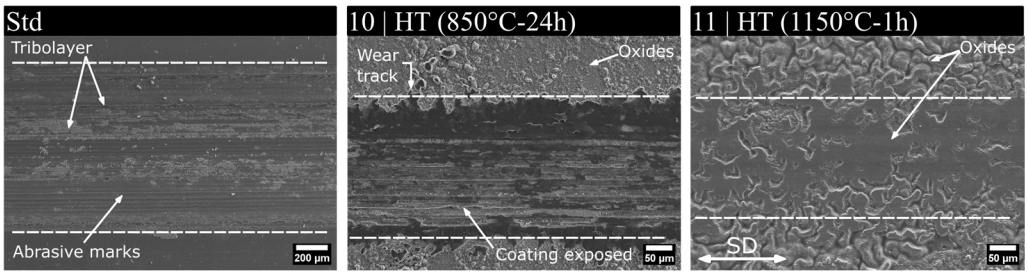


Figure 8. Top view of wear tracks taken with SE. Condition number is stated as the top left of each picture.

3.3.1. Spray Parameters

The standard spraying parameters (Table 1-A) produced a dense Stellite 6 coating with oxidized regions throughout the microstructure. In contrast, the second set of spraying conditions used a higher fuel-to-oxygen ratio (Table 1-B), which reduced the available oxygen for interaction with the powder during the high-velocity oxy-fuel deposition process [34]. This decrease in oxygen exposure consequently led to a reduction in the oxide regions

within the Stellite 6 coating, as shown in Figure 9. The oxide regions produced under the standard spraying parameters are clearly highlighted in Figure 9a. In contrast, after the fuel-to-oxygen ratio was increased, the microstructure shown in Figure 9b exhibited only the metallic splats. This alternative coating was also dense but was more porous (3%) than the standard coating (1%).

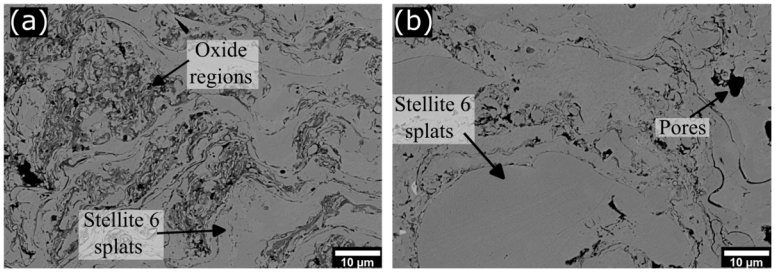


Figure 9. Cross-section of coatings sprayed with (**a**) standard parameters A and (**b**) fuel reach parameters B.

Despite the reduction in oxide regions achieved, the modified spraying parameters did not improve the wear rate of the Stellite 6 coating after the test was repeated a second time. In fact, the average wear rate at the standard conditions was lower than the conditions with decreased oxide content ($162 \pm 12.6 \times 10^{-6}$ mm^3/Nm and $180 \pm 7.9 \times 10^{-6}$ mm^3/Nm, respectively). As shown in the high-magnification images of the wear track (Figure 10), the Std1 conditions produced a region covered by various oxide morphologies, including thin, smeared oxides and rough patches of tribolayers. In areas free of tribolayers, as seen with the Std2 conditions, significant oxidation was observed in the intersplat regions. In contrast, for condition 1, the oxides at the intersplats were less prevalent, and the tribolayer had a predominantly rough morphology, suggesting that the presence of oxides (in the absence of hard intermetallics compared with bulk samples) played a role in the wear behavior of the HVOF-sprayed Stellite 6 coatings.

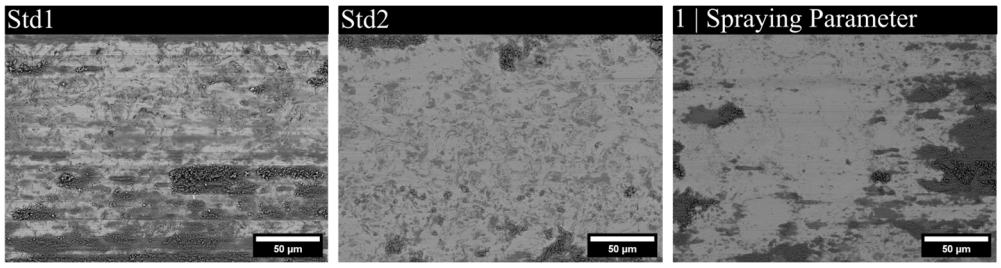


Figure 10. Top view of the wear tracks, Std1, Std2, and condition 1.

3.3.2. Testing Temperature

Temperature is an essential parameter influencing the wear performance of Stellite 6 alloy. At temperatures below the severe-to-mild wear transition, the mechanical properties of the material are affected by thermal softening, which can reduce the material's hardness and resistance to wear [33]. Figure 11 highlights the oxidative wear occurring on the coatings. While these oxides presented a rounder shape, the oxide patches formed at 300 °C were preferentially deformed in the sliding direction. As a result, the wear rate at 100 °C was lower than at 300 °C, where the material experienced less thermal softening (Figure 7). The temperature-dependent wear behaviors are comparable to results from bulk material studies, where the Vm100/300 ratio (the ratio of wear rates at 100 °C and 300 °C) indicates the alloy's ability to form a protective tribolayer at higher temperatures. For the current Stellite 6 coating, this ratio was 0.54, suggesting that this coating did not form a sufficiently

protective tribolayer at 300 °C to mitigate the increased wear rate. In contrast, in other studies where a more effective protective layer formed, the Vm100/300 ratio was higher than 1, indicating lower wear at the elevated temperature (5 for HS25 alloy [8]).

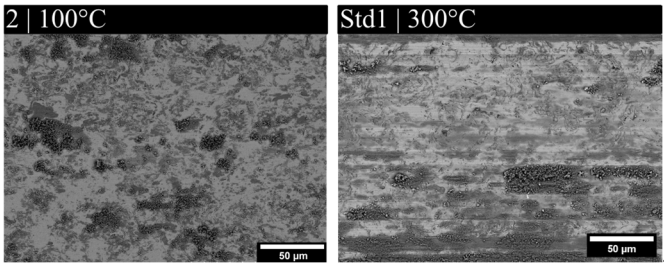


Figure 11. Top view of the wear tracks, conditions 2 and Std1.

3.3.3. Applied Load

The formation of a protective tribolayer is a tribo-sintering process that requires the application of sufficient contact stress. Normal loads of 1 N, 5 N, and 10 N applied during the wear testing corresponded to average Hertzian contact stresses of 0.6, 1.03, and 1.3 GPa, respectively. Previous studies have shown that at temperatures below the severe-to-mild wear transition, the material's volume loss tends to increase with higher applied loads since higher contact stresses can disrupt the formation and stability of the protective tribolayer. A similar trend can be observed in Figure 12a, where the wear tracks become wider and deeper as the load increases. Despite the differences in wear track size, the three loading conditions exhibited comparable wear rates (Figure 7), suggesting that the tribolayers that were formed during wear, while disrupted by the higher loads, were still able to provide the same level of protection against wear. Under all three load levels, similar wear mechanisms were observed, characterized by patchy tribolayers across the wear track and abrasive marks (Figure 13), indicating that the current contact stresses at 300 °C did not provide the conditions to form tribolayers that fully protect the surface.

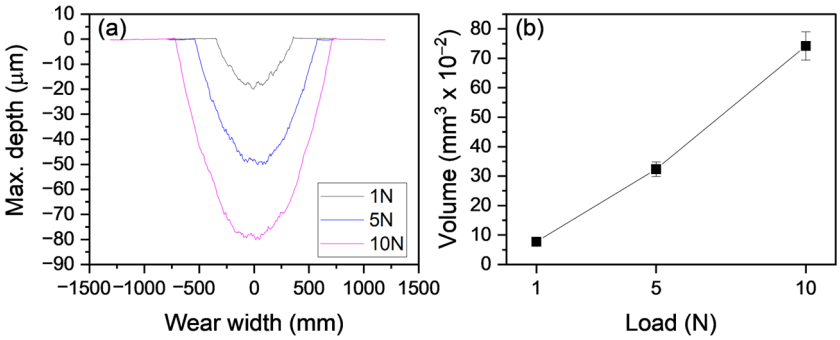


Figure 12. (**a**) Maximum wear depth (wear size) and (**b**) wear volume per load.

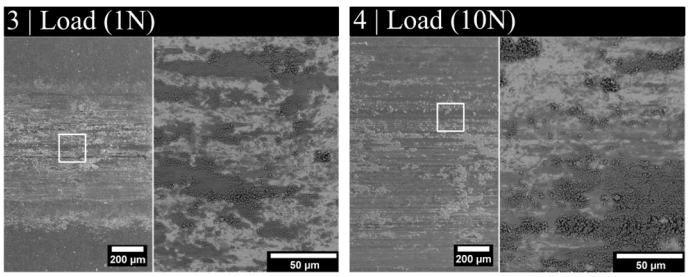


Figure 13. Top view of the wear tracks, conditions 3 and 4; left image taken with SE and right image with BSE.

3.3.4. Distance

The wear behavior was tested across a range of sliding distances, each corresponding to a different test duration. As shown in Figure 14, more extensive tribolayer coverage was evident after 800 m of sliding, indicating that the tribolayer formation was a gradual process that required a certain sliding distance (or time) to develop. However, even after doubling the sliding distance to 1600 m, the wear mechanisms remained similar, featuring both abrasive and oxidative wear. While the wear rate decreased with increasing distance, material removal continued up to 1600 m, suggesting that the tribolayer was not fully protective. The high variability in wear rate measurements (six repeats) at 3200 m of sliding suggests the material might have been in the transition zone between severe and mild wear [11,12,39]. Although tribolayers were observed on the samples in earlier stages of the testing (between 100 and 1600 m), these were continuously removed by the sliding motion and were unable to fully protect the underlying coating. The volume loss between this interval increased with the distance. However, the volume loss was similar between 1600 m and 3200 m of sliding distance (101 $\pm$ 19 and 97 $\pm$ 6 $\times$ 10^2 mm^3, respectively). A more protective tribolayer developed between 1600 and 3200 m of sliding distance, and the sample worn for 3200 m exhibited a more continuous layer (see Figure 15).

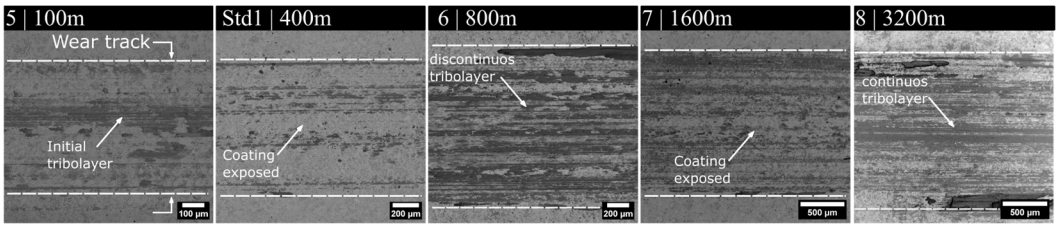


Figure 14. Top view of the wear tracks after 100 m, 400 m, 800 m, 1600 m and 3200 m under different magnifications.

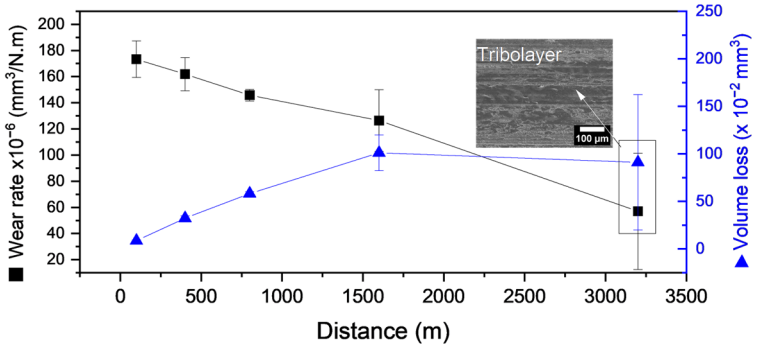


Figure 15. Wear rate and volume loss per distance.

3.3.5. Heat Treatment

Three heat treatment conditions were investigated under conditions 9 to 11. Condition 9, 600 °C for 2 h, enhanced oxidation primarily at the splat boundaries (Figure 16), similar to the as-sprayed state (Figure 1b). These oxides were more likely to smear during wear, and the wear rate was comparable to the standard condition, indicating no improvement in wear resistance (Figure 16, edge of wear track is marked with a dotted line). Condition 10, 850 °C for 24 h, resulted in complete surface coverage by oxides and a significantly decreased, more stable coefficient of friction (Figures 5 and 16). However, these oxides were largely removed from the surface during wear, exposing the underlying coating and revealing abrasive marks. Consequently, wear resistance was not improved.

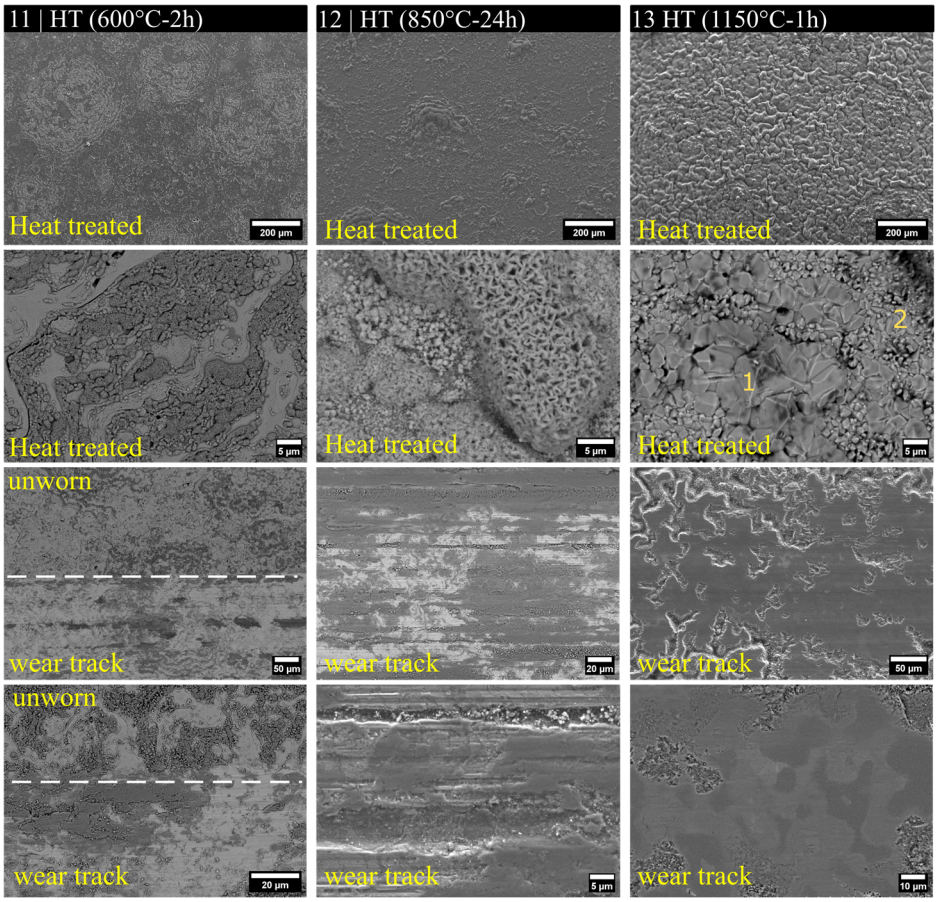


Figure 16. Top view of the coating after heat treatment (**top images**) and after wear test (**lower images**) with low and high magnification. EDS analysis of points 1 and 2 is presented in Table 4.

Table 4. Chemical composition analysis of the sample after heat treatment at 1150 °C and 1 h, detailed in Figures 16 and 17.

Element	1	2	3
Co	22.7	12.6	0.8
Cr	47.4	58.1	67.6
W	-	-	-
C	1.7	1.9	1.6
O	28.2	27.4	30

In contrast, the heat treatment of condition 11, 1150 °C for 1 h produced a coating covered in a dense network of oxides of cobalt and chromium (Table 4-point 1 and 2). The presence of these oxides reduced the average coefficient of friction with a steadier state (Figure 5). Importantly, this condition exhibited the lowest wear rate among all the evaluated conditions, for which two tests were performed for repeatability (Figure 7). Micrographs of the wear track revealed a smooth, smeared oxide morphology on the wear track, suggesting the formation of a protective oxide tribolayer that contributed to the improved wear performance (Figure 16).

A cross-section of the heat-treated sample (before wear) revealed an oxide layer with a maximum thickness of 8 µm, with the main element being chromium (Figure 17 and Table 4-point 3), suggesting that the oxide layer was formed mainly of chromium oxide with a top layer of mixed (Co-Cr) oxides [38]. The cross-section of the worn surface was obtained using a FIB by thinning the sample prior to the analysis with the STEM (Figure 17). During this process, the electron beam damaged the sample, removing part of the platinum

protection that had been placed on the top of the sample. The extended time required for thinning the sample suggests high hardness in the worn region. Meanwhile, no cracks were observed on the cross-section, highlighting the high toughness of the oxide layers. The cross-section of the worn sample's tribolayer confirms the presence of a thick layer of Cr-oxide (EDS-mapping No. 4 and SAED pattern No. 7). On top of the Cr-O layer, a top layer was identified consisting of refined grains of Co and Cr oxides (binary and ternary oxides). However, it was hard to estimate the extension of the refined-oxide region within the wear track due to the beam damage.

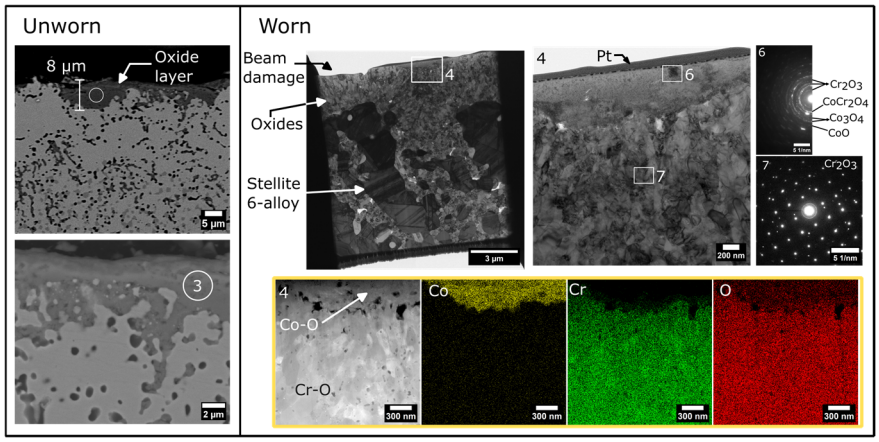


Figure 17. Heat-treated sample cross-section before (**left**) and after (**right**) wear tests. EDS analysis of point 3 is presented in Table 4. SAED patterns (6 and 7) and EDS mapping are taken from the marked region 4.

4. Conclusions

This study provides valuable insights into the wear performance of HVOF-sprayed Stellite 6 coatings at 300 °C. The wear behavior of the coating was comparable under most testing conditions, with values between 1×10^{-4} and 2×10^{-4} $mm^3/N{\cdot}m$. The wear performance was significantly improved using a heat treatment; crucially, it reduced the wear rate by more than 90%, reaching values in the order of 10^{-6} $mm^3/N{\cdot}m$. The most effective heat treatment involved exposure to 1150 °C for one hour, resulting in a dense oxide network that facilitated the formation of a protective tribolayer and minimized wear. Otherwise, the coating in as-spray condition required a large sliding distance (between 1600 m and 3200 m) to properly form the glaze layer, after which the volume loss reached a plateau. However, further testing is needed to confirm the long-term stability of this tribolayer and whether it can withstand prolonged sliding without the need for heat treatment. These results will help guide the development of more wear-resistant Stellite 6 coatings for high-temperature applications.

Author Contributions: Conceptualization, A.I.E., M.M., P.S., C.M. and R.R.C.; methodology, A.I.E., P.S., C.M. and R.R.C.; investigation, A.I.E.; resources, M.M., C.M. and R.R.C.; writing—original draft preparation, A.I.E.; writing—review and editing, R.R.C.; visualization, A.I.E.; supervision, C.M. and R.R.C.; project administration, M.M., C.M. and R.R.C.; funding acquisition, M.M., P.S., C.M. and R.R.C. All authors have read and agreed to the published version of the manuscript.

Funding: This research was funded by the Natural Sciences and Engineering Research Council (NSERC) (project number CRDPJ 530409-18) and the Consortium for Research and Innovation in Aerospace in Quebec (CRIAQ) (project number MANU-1719), and a McGill Engineering Doctoral Award (MEDA) and CONAHCyT (CVU-638758) awarded to A.I.E.

Data Availability Statement: The raw data supporting the conclusions of this article will be made available by the authors upon request.

Acknowledgments: The authors would like to acknowledge the support of Fadhel Ben Ettouil with the coating deposition; Weawkamol Leelapornisit and David Liu for STEM sample preparation and imaging; and Eutectic Canada for supplying the powders used in this project.

Conflicts of Interest: Mary Makowiec is an employee of Pratt & Whitney. The remaining authors declare that the research was conducted in the absence of any commercial or financial relationships that could be construed as a potential conflict of interest.

Abbreviations

The following abbreviations are used in this manuscript:

HVOF	High-velocity oxygen fuel
COF	Coefficient of friction
Std	Standard
FCC	Faced-centered cubic

References

1. Coutsouradis, D.; Davin, A.; Lamberigts, M. Cobalt-based superalloys for applications in gas turbines. *Mater. Sci. Eng.* **1987**, *88*, 11–19. [CrossRef]
2. Crook, P.; Levy, A. Cobalt-Base Alloys. In *Corrosion Tests and Standards: Application and Interpretation*, 2nd ed.; ASTM MANUAL SERIES MNL; ASTM International: West Conshohocken, PA, USA, 1995; pp. 486–492.
3. Davis, J.R.; American Society for Metals International Handbook Committee. *Nickel, Cobalt, and Their Alloys*; ASM International: Materials Park, OH, USA, 2000.
4. Baboian, R. *Corrosion Tests and Standards: Application and Interpretation*; ASTM International: West Conshohocken, PA, USA, 2005.
5. Antony, K.C. Wear-Resistant Cobalt-Base Alloys. *JOM* **1983**, *35*, 52–60. [CrossRef]
6. Eastman, J.W. Book Review: Stellite: A History of the Haynes Stellite Company, 1912–1972. *Bus. Hist. Rev.* **1975**, *49*, 272–273. [CrossRef]
7. Stott, F.H.; Stevenson, C.W.; Wood, G.C. Friction and wear properties of Stellite 31 at temperatures from 293 to 1073K. *Met. Technol.* **1977**, *4*, 66–74. [CrossRef]
8. Viat, A.; Dreano, A.; Fouvry, S.; De Barros Bouchet, M.-I.; Henne, J.-F. Fretting wear of pure cobalt chromium and nickel to identify the distinct roles of HS25 alloying elements in high temperature glaze layer formation. *Wear Part B* **2017**, *376–377*, 1043–1054. [CrossRef]
9. Birol, Y. High temperature sliding wear behaviour of Inconel 617 and Stellite 6 alloys. *Wear* **2010**, *269*, 664–671. [CrossRef]
10. Blau, P. Elevated-Temperature Tribology of Metallic Materials. *Tribol. Int.* **2010**, *43*, 1203–1208. [CrossRef]
11. Dreano, A.; Fouvry, S.; Guillonneau, G. A combined friction energy and tribo-oxidation formulation to describe the high temperature fretting wear response of a cobalt-based alloy. *Wear Part A* **2019**, *426–427*, 712–724. [CrossRef]
12. Dreano, A.; Fouvry, S.; Guillonneau, G. Understanding and formalization of the fretting-wear behavior of a cobalt-based alloy at high temperature. *Wear* **2020**, *452–453*, 203297. [CrossRef]
13. Dreano, A.; Fouvry, S.; Sao-Joao, S.; Galipaud, J.; Guillonneau, G. The formation of a cobalt-based glaze layer at high temperature: A layered structure. *Wear* **2019**, *440–441*, 203101. [CrossRef]
14. Huang, C.; Zou, B.; Guo, P.; Liu, Y.; Huang, C.; Wang, J. Sliding behavior and wear mechanism of iron and cobalt-based high-temperature alloys against WC and SiC balls. *Int. J. Refract. Met. Hard Mater.* **2016**, *59*, 40–55. [CrossRef]
15. Korashy, A.; Attia, H.; Thomson, V.; Oskooei, S. Characterization of fretting wear of cobalt-based superalloys at high temperature for aero-engine combustor components. *Wear* **2015**, *330–331*, 327–337. [CrossRef]
16. Pauschitz, A.; Roy, M.; Franek, F. Mechanisms of sliding wear of metals and alloys at elevated temperatures. *Tribol. Int.* **2008**, *41*, 584–602. [CrossRef]
17. Viat, A.; De Barros Bouchet, M.-I.; Vacher, B.; Le Mogne, T.; Fouvry, S.; Henne, J.-F. Nanocrystalline glaze layer in ceramic-metallic interface under fretting wear. *Surf. Coat. Technol.* **2016**, *308*, 307–315. [CrossRef]
18. Viat, A.; Guillonneau, G.; Fouvry, S.; Kermouche, G.; Sao Joao, S.; Wehrs, J.; Michler, J.; Henne, J.-F. Brittle to ductile transition of tribomaterial in relation to wear response at high temperatures. *Wear* **2017**, *392–393*, 60–68. [CrossRef]
19. Wood, P.D.; Evans, H.E.; Ponton, C.B. Investigation into the wear behaviour of Stellite 6 during rotation as an unlubricated bearing at 600 °C. *Tribol. Int.* **2011**, *44*, 1589–1597. [CrossRef]
20. Dreano, A.; Baydoun, S.; Fouvry, S.; Nar, S.; Alvarez, P. Influence of a pre-existing glaze layer on the fretting-wear response of HS25 cobalt-based alloy subjected to various temperature conditions. *Wear* **2022**, *488–489*, 204144. [CrossRef]

21. Baydoun, S.; Moul-El-Ksour, F.Z.; Fouvry, S.; Guillonneau, G.; Pereira, J.C.; Santos, F.; Niklas, A.; Lopez-Ruiz, P.; Vega, J.; Rocchi, J. Tribological investigation of new self-fluxing nickel alloys for high temperature application: The effect of silicon distribution on glaze layer formation. *Wear* **2025**, *564–565*, 205631. [CrossRef]
22. Manoj, A.; Verma, P.C.; Narala, S.K.R.; Saravanan, P.; Tiwari, S.K.; Joshi, S. High-temperature tribological evaluation of cobalt-based laser cladded disc for automotive brake systems. *Ceram. Int.* **2024**, *50*, 54458–54472. [CrossRef]
23. Huang, H.; Wang, W.; Shan, Y.; Yi, G.; Wan, S.; Zhang, G.; Du, X.; Ma, F. Influences of counterparts on the high-temperature tribological properties and glaze layer formation of pre-oxidized cobalt-based alloys. *Wear* **2024**, *544–545*, 205260. [CrossRef]
24. Zhen, J.; Han, Y.; Yuan, L.; Jia, Z.; Zhang, R. Investigating Influence of Mo Elements on Friction and Wear Performance of Nickel Alloy Matrix Composites in Air from 25 to 800 °C. *Lubricants* **2024**, *12*, 396. [CrossRef]
25. Wei, C.; Yang, L.; Duan, R.; Chu, K.; Ren, F. Sliding wear-induced compositional lamination in a VCoNi alloy at elevated temperatures, and its implications for reduced friction and wear. *Acta Mater.* **2024**, *277*, 120171. [CrossRef]
26. Frenk, A.; Kurz, W. Microstructural effects on the sliding wear resistance of a cobalt-based alloy. *Wear* **1994**, *174*, 81–91. [CrossRef]
27. Asl, S.K.; Sohi, M.H.; Hokamoto, K.; Uemura, M. Effect of heat treatment on wear behavior of HVOF thermally sprayed WC-Co coatings. *Wear* **2006**, *260*, 1203–1208. [CrossRef]
28. Bolelli, G.; Cannillo, V.; Lusvarghi, L.; Montorsi, M.; Mantini, F.P.; Barletta, M. Microstructural and tribological comparison of HVOF-sprayed and post-treated M–Mo–Cr–Si (M=Co, Ni) alloy coatings. *Wear* **2007**, *263*, 1397–1416. [CrossRef]
29. Bolelli, G.; Lusvarghi, L. Heat Treatment Effects on the Tribological Performance of HVOF Sprayed Co-Mo-Cr-Si Coatings. *J. Therm. Spray Technol.* **2006**, *15*, 802–810. [CrossRef]
30. Bolelli, G.; Lusvarghi, L. Tribological properties of HVOF as-sprayed and heat treated Co–Mo–Cr–Si coatings. *Tribol. Lett.* **2006**, *25*, 43–54. [CrossRef]
31. Houdková, Š.; Smazalová, E.; Pala, Z. Effect of Heat Treatment on the Microstructure and Properties of HVOF-Sprayed Co-Cr-W Coating. *J. Therm. Spray Technol.* **2016**, *25*, 546–557. [CrossRef]
32. Wang, Y.; Zhao, X.; Hao, E.; Bu, Z.; An, Y.; Zhou, H.; Chen, J. High temperature induced "glaze" layer formed in HVOF-sprayed NiCrWMoCuCBFe coating and its wear reduction mechanism. *Friction* **2022**, *10*, 1424–1438. [CrossRef]
33. Islas Encalada, A.; Alidokht, S.A.; Sharifi, N.; Stoyanov, P.; Makowiec, M.; Moreau, C.; Chromik, R.R. Wear behavior of HVOF sprayed cobalt-based composite coatings reinforced with Cr_3C_2. *Wear* **2024**, *546–547*, 205310. [CrossRef]
34. Patel, P.; Munagala, V.N.V.; Sharifi, N.; Roy, A.; Alidokht, S.A.; Harfouche, M.; Makowiec, M.; Stoyanov, P.; Chromik, R.R.; Moreau, C. Influence of HVOF spraying parameters on microstructure and mechanical properties of FeCrMnCoNi high-entropy coatings (HECs). *J. Mater. Sci.* **2024**, *59*, 4293–4323. [CrossRef]
35. Kato, H.; Komai, K. Tribofilm formation and mild wear by tribo-sintering of nanometer-sized oxide particles on rubbing steel surfaces. *Wear* **2007**, *262*, 36–41. [CrossRef]
36. Hager, C.H.; Hu, J.; Muratore, C.; Voevodin, A.A.; Grandhi, R. The mechanisms of gross slip fretting wear on nickel oxide/Ti6Al4V mated surfaces. *Wear* **2010**, *268*, 1195–1204. [CrossRef]
37. Yao, M.X.; Wu, J.B.C.; Xu, W.; Liu, R. Metallographic study and wear resistance of a high-C wrought Co-based alloy Stellite 706K. *Mater. Sci. Eng. A* **2005**, *407*, 291–298. [CrossRef]
38. Lund, C.H.; Wagner, H.J. *Oxidation of Nickel- and Cobalt-Base Superalloys*; Defense Metals Information Center, Battelle Memorial Institute: Columbus, OH, USA, 1965.
39. Dréano, A.; Fouvry, S.; Guillonneau, G. A tribo-oxidation abrasive wear model to quantify the wear rate of a cobalt-based alloy subjected to fretting in low-to-medium temperature conditions. *Tribol. Int.* **2018**, *125*, 128–140. [CrossRef]

Disclaimer/Publisher's Note: The statements, opinions and data contained in all publications are solely those of the individual author(s) and contributor(s) and not of MDPI and/or the editor(s). MDPI and/or the editor(s) disclaim responsibility for any injury to people or property resulting from any ideas, methods, instructions or products referred to in the content.